

Article

Structure Defects and Photovoltaic Properties of TiO₂:ZnO/CuO Solar Cells Prepared by Reactive DC Magnetron Sputtering

Grzegorz Wisz ^{1,*}, Paulina Sawicka-Chudy ¹, Andrzej Wal ², Maciej Sibiński ³, Piotr Potera ¹, Rostyslaw Yavorskyi ⁴, Lyubomyr Nykyruy ⁴, Dariusz Płoch ¹, Mariusz Bester ², Marian Cholewa ² and Olena M. Chernikova ⁵

¹ Institute of Materials Engineering, College of Natural Science, University of Rzeszow, 1 Pigionia St., 35-317 Rzeszow, Poland

² Institute of Physics, College of Natural Sciences, University of Rzeszow, 1 Pigionia St., 35-317 Rzeszow, Poland

³ Department of Semiconductor and Optoelectronic Devices, Lodz University of Technology, Wolczanska St. 211/215, 90-924 Lodz, Poland

⁴ Department of Physics and Chemistry of Solids, Vasyl Stefanyk Precarpathian National University, T. Shevchenko St. 57, 76018 Ivano-Frankivsk, Ukraine

⁵ Department of Higher Mathematics and of Physics, Faculty of Information Technology, Kryvyi Rih National University, 11 Vitaliy Matusevych St., 50027 Kryvyi Rih, Ukraine

* Correspondence: gwisz@ur.edu.pl

Abstract: The problem of copper diffusion in semiconductor devices has been known for several decades as copper has been used as an interconnecting (bonding) metal and has been intensively studied due to its high diffusion coefficient. The influence of the intensive diffusion of copper, depending on the technology of the deposition regimes, has been investigated in thin-film solar cells based on copper, zinc, and titanium oxides obtained by DC-reactive magnetron sputtering. The observed effect significantly changes the structure of the CuO films and affects the properties of the TiO₂:ZnO/CuO photocell. The composition of the layers and the copper diffusion in the photocells were studied using a cross-section obtained by scanning electron microscopy (SEM). The influence of the copper diffusion in the layers on the current–voltage (I-V) and power–voltage (P-V) characteristics and optical properties was investigated. The photoelectric behavior of two structures of thin-film solar cells was confirmed through $-V$ research. The values of the open-circuit voltage (V_{OC}) and short-circuit current density (J_{SC}) of photovoltaic devices reached $(11 \div 15)$ mV and $(6.1 \div 6.8)$ μ A, respectively. Furthermore, the P_{max} , FF, RS, and RSH values were calculated and analyzed. The difference in the composition of the upper layer of the structure caused changes in the reflection spectra in the wavelength range of 190–2500 nm and, depending on the wavelength, varies in the range of 0–27%.

Keywords: copper diffusion; PV applications; thin film solar cells; DC sputtering; structural defects



Citation: Wisz, G.; Sawicka-Chudy, P.; Wal, A.; Sibiński, M.; Potera, P.; Yavorskyi, R.; Nykyruy, L.; Ploch, D.; Bester, M.; Cholewa, M.; et al. Structure Defects and Photovoltaic Properties of TiO₂:ZnO/CuO Solar Cells Prepared by Reactive DC Magnetron Sputtering. *Appl. Sci.* **2023**, *13*, 3613. <https://doi.org/10.3390/app13063613>

Academic Editor: José A. Jiménez

Received: 20 February 2023

Revised: 5 March 2023

Accepted: 8 March 2023

Published: 11 March 2023



Copyright: © 2023 by the authors. Licensee MDPI, Basel, Switzerland. This article is an open access article distributed under the terms and conditions of the Creative Commons Attribution (CC BY) license (<https://creativecommons.org/licenses/by/4.0/>).

1. Introduction

Over the past few decades, copper has been used as an interconnecting metal in semiconductor technology. It replaces the previously used aluminum. However, it has been observed that the use of copper leads to its diffusion into the active regions of semiconductor devices. This is because copper atoms have the highest diffusion coefficient values in silicon (germanium) compared to other metals [1]. The problem of copper diffusion in semiconductors and methods for its prevention have attracted the interest of researchers. One technique is to use materials such as TiN [2], Ta/TaN [3], TaC [4], and MnSiO₃ [5]. In addition, amorphous carbon can be used as a barrier against Cu diffusion in Cu/SiO₂/Si systems [6]. A review of contemporary copper-diffusion-blocking layers and techniques for their production can be found in the work of Li et al. [7]. The problem of preventing Cu

diffusion also concerns the applications of semiconductors in solar cells, where copper is used to form contacts [8].

The problem of the diffusion mechanism, its speed, and its temperature dependencies has been considered for a long time. Various techniques were used in these studies to experimentally track the diffusion of copper atoms in various materials, including metal oxides. The paper by Peterson and Wiley [9] presented an extensive study of the diffusion of radioactive copper in Cu_2O . The sample was prepared in a polycrystalline form and tested at temperatures of 700–1153 °C for various partial pressures of oxygen (greater than 10^{-6} atm). It was shown that the self-diffusion coefficient depends on both these parameters, i.e., the partial pressure of oxygen and the temperature (according to the Arrhenius equation). The paper also presented a model of defects in the Cu_2O lattice, which was adjusted to the results of the measurement of the diffusion and electrical conductivity of copper oxides. By analyzing the dependence of the diffusion coefficient on the oxygen pressure, the authors showed that the diffusion of copper cations takes place through copper vacancies, i.e., singly charged and neutral copper vacancies.

The determination of the diffusion coefficient D of copper in the copper oxide Cu_2O was also covered by Moor et al. [10]. The research method was similar to the work of Peterson [9], that is, the penetration of radioactive copper into the copper oxide layer was monitored. The linear dependence of the $\ln(D)$ as a function of the reciprocal temperature in the air atmosphere was found.

It is also possible to determine the diffusion coefficient by other methods, e.g., from oxidation kinetics, if only the scale is compact, single-phase, and is formed by the diffusion of one type of species. In [11], the diffusion coefficient of Cu in Cu_2O was determined from measurements of the oxidation kinetics, which were determined thermogravimetrically. Similar studies were carried out by Iguchi et al. [12]. In addition, they presented a detailed description of the diffusion of metal cations and oxygen anions in the investigated copper oxide.

Experimentally, Cu_2O oxidation can be studied using transmission optical spectroscopy [13]. On this basis, the change in the energy gap during oxidation was assessed, allowing for the determination of the fraction of CuO and the rate of phase change from Cu_2O to CuO. In the initial stage of this process, the rate of oxidation is logarithmic. It later changes to parabolic, and at high temperatures it becomes exponential. Studies have also shown that the oxidation process takes place in a planar and uniform front, in contrast to copper oxidation, where grain boundaries are the main oxidation pathway [13].

XRD is another method for studying the oxidation of Cu_2O to CuO. In the work of Unutulmazsoy et al. [14], due to the normalized integration of the peak areas of the XRD signal, it was possible to determine how changes in the oxide phases occur over time. The diffusion rate of Cu ions in CuO oxide was shown to be much lower than in Cu_2O ; therefore, at lower temperatures, e.g., 300 °C, the diffusion is too slow for a thick CuO layer to form in the Cu_2O layer formed from Cu oxidation. The process of oxide transformation is related to the movement of Cu ions toward the upper edge of the Cu_2O layer through cation vacancies.

Lee et al. [15] also studied the course of copper oxidation processes but at relatively low temperatures of below 300 °C. This work confirmed that during oxidation, a Cu_2O layer first appears, and on its outer surface, even at low temperatures, a thin CuO layer forms. The authors also proposed a passivation process by heating a sample for 3 min in a N_2 atmosphere at 600 °C, which slowed the oxidation process by an order of magnitude.

Cuprous oxide (Cu_2O) and cupric oxide (CuO) can be produced in many ways, including low-temperature processes. Article [16] describes the process of obtaining Cu_2O by converting the CuI layer in a NaOH solution, and the further oxidation of the compound obtained at 250 °C led to the formation of the CuO layer. These layers were used as hole-transporting materials in perovskite-based solar cells, leading to high efficiencies.

Another technique for obtaining copper oxide can be pyrolysis. This method also allows doping the CuO oxide with metals; for example, manganese [17]. Such doping leads

to a change in the properties of the oxide, including the control of the energy gap width, which may make this material advantageous from the point of view of optoelectronic applications. An interesting solution that increases the efficiency of photovoltaic cells is a cogeneration system that combines the generation of electricity with the simultaneous production of hydrogen and an additional mechanism for obtaining thermal energy, which is generated during the operation of photovoltaic panels. This combination ensures a better use of solar energy. Techniques to optimize the parameters that affect the operating conditions of the hybrid device are presented in [18]. Elaziz et al. [19], who provided a fairly extensive review of research in this field, presented the analysis of such systems both on the model and on the experimental side. Interestingly, the elements used to optimize the operating parameters of the systems were determined using artificial intelligence.

A detailed discussion on the formation of copper oxide layers and the role of copper and oxygen diffusion in them can be found in the paper by Košíček et al. [20]. The authors also described the rate of oxidation processes at different temperatures (in the range from 400 to 700 °C). However, by performing tests using scanning and transmission electron microscopes, the authors also described the morphology of the cross-section of the layers. These microstructural studies revealed that randomly oriented, columnar Cu₂O grains first appear during annealing, followed by CuO grains oriented in preferred directions. At the Cu/Cu₂O boundary, the grains were smaller than at a greater distance from this boundary and have an equiaxed character. In turn, on the upper side of the Cu₂O layer, small CuO grains with strong texturization were observed. Surfaces that separate individual layers have a temperature-dependent morphology. At low temperatures, the surface between the oxide layers did not show visible losses or cracks, while annealing at high temperature caused cracks and holes at the Cu/Cu₂O interface. This caused the diffusion of copper ions towards the oxides to cease.

In the process of the deposition of thin-film heterostructures, the surface diffusion process, which is the main process, makes it possible to control the uniformity of the film in the horizontal (lateral) and normal directions. Transport from the vapor phase (layer growth) controls the uniformity of the film, which further affects the electrical, optical, and physicochemical properties of the obtained heterostructures. The growth of a homogeneous structure can be supported only when a sufficient number of atomic transitions between the layers of the film is ensured during the growth process. This means that the dropped atom at the top of the growth island with a high probability can move to the lower layer where the potential energy is lower. Therefore, the study of the structure in the cross-section makes it possible to evaluate the processes of self-organization and growth mechanisms depending on the conditions of deposition.

In this paper, the complex influence of the copper diffusion mechanism on the properties of thin-film photovoltaic cells based on copper, zinc, and titanium oxides produced by magnetron sputtering was examined for the first time. Diffusion, which depends on the production conditions, affects the structure of the CuO layer and therefore the photovoltaic properties of the entire TiO₂:ZnO/CuO structure. In the comprehensive research on the process flow, the mechanical, electrical and optical parameters of the multilayers structure are examined. Novel explanation of some observed phenomena are proposed in addition to some guidelines for further ameliorations of the production process.

2. Materials and Methods

Preparation of TiO₂:ZnO/CuO

TiO₂:ZnO/CuO solar cells were prepared using reactive, direct-current magnetron sputtering (DC-MS). Details of the sputtering conditions and the approximate value of the thickness of the TiO₂:ZnO and CuO layers are shown in Tables 1 and 2. More details on the method and the apparatus used can be found in the Supplementary Materials. The substrate temperature during layer growth was kept at 300 °C. The deposition process was as follows. First, thin films of n-type TiO₂:ZnO were deposited on glass substrates with ITO (indium tin oxide) with dimensions of 10 × 10 × 1.1 mm and commercial silicon plates

(N-type Si, 100), using ZnOTiO₂ 4–3 at% (Z1-9057-D3 commercial target from Testbourne) for Samples #14, #15, and #18 and the self-produced Ti:ZnO target for Samples #26 and #27 (see the preparation of the Ti-ZnO target in [21]). Next, a Cu buffer layer, a p-type copper oxide absorber layer, and a thin Cu film were grown successively using a Cu target (99.995% from Kurt J. Lesker Company). For the Cu buffer layer production in particular, the following process parameters and procedures were used:

- For Sample #14: deposition time 10 s, argon flow rate 1 cm³/s; the magnetron shutter was closed, flows were set for deposition of the CuO layer, the plasma beam was stabilized for 20 s with the shutter closed, and the deposition of the CuO layer began;
- For Samples #15 and #18: no Cu buffer between TiO₂:ZnO and CuO was used;
- For Sample #26: deposition time 5 s, argon flow 4 cm³/s; the oxygen flow was switched on, and the CuO layer deposition was started smoothly,
- For Sample #27: deposition time 5 s, argon flow 1 cm³/s; the oxygen flow was switched on, the argon flow was set to 1 cm³/s, and the CuO layer deposition was started smoothly.

Table 1. Growth parameters of the TiO₂ + ZnO window layer.

	#14	#15	#18	#26	#27
Time [min]	30	40	30	20	25
Power [W]	100	100	100	100	100
Pressure [mbar]	9.89×10^{-3}	9.89×10^{-3}	9.89×10^{-3}	8.99×10^{-3}	8.99×10^{-3}
Distance between the source and substrate [mm]	58	58	58	58	58
Oxygen flow rate [cm ³ /s]	3.5	3.5	3.5	3	2.5
Argon flow rate [cm ³ /s]	0.5	0.5	0.5	1	1
Substrate temperature [°C]	300	300	350	300	300
Thickness [nm]	86	43	57	245	354

Table 2. Growth parameters of the CuO absorber layer.

	#14	#15	#18	#26	#27
Time [min]	30	30	30	30	30
Power [W]	70	70	70	70	70
Pressure [mbar]	9.23×10^{-3}	8.75×10^{-3}	9.41×10^{-3}	1.05×10^{-2}	1.11×10^{-2}
Distance between the source and substrate [mm]	58	58	58	58	58
Oxygen flow rate [cm ³ /s]	3.5	3.5	3.5	3.5	3.5
Argon flow rate [cm ³ /s]	0.5	0.5	0.5	1	1
Substrate temperature [°C]	300	300	300	300	300
Thickness [nm]	747	723	650	1654	1487

The remaining process parameters were the same for the CuO layers; see Table 2. A scheme of the TiO₂:ZnO/CuO thin-film solar cells and a real view of TiO₂:ZnO/CuO/Cu₂O Sample #27 are shown in Figure 1a,b.

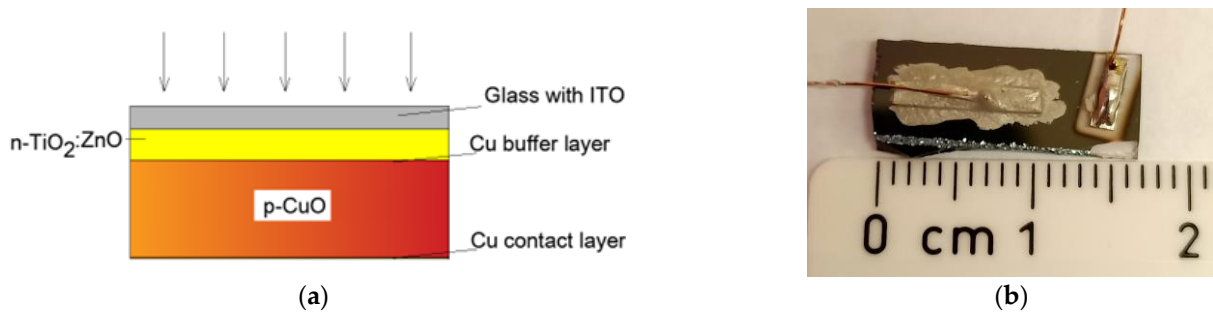


Figure 1. (a) Scheme of the TiO₂:ZnO/CuO thin-film solar cells; (b) real view of the sample.

Finally, the following procedure and parameters were used to deposit the back-contact copper electrode:

- For Samples #14, #15: the magnetron shutter was closed after CuO deposition, the argon flow was set to 1 cm³/s, the plasma beam was stabilized for 20 s with the shutter closed, and the deposition of the Cu layer by 60 s was initiated;
- For Sample #18: the oxygen flow was closed after the CuO deposition (the argon flow stayed at 1 cm³/s), and the Cu layer deposition was started smoothly by 60 s;
- For Sample #26: the oxygen flow was closed after CuO deposition (the argon flow stayed at 1 cm³/s), and the Cu layer deposition was started smoothly by 20 s,
- For Sample #27: the oxygen flow was closed after CuO deposition, the argon flow was set to 4 cm³/s, and the Cu layer deposition was started smoothly by 20 s.

The process flow diagram for the solar cell fabricated in this study is shown in Figure 2.

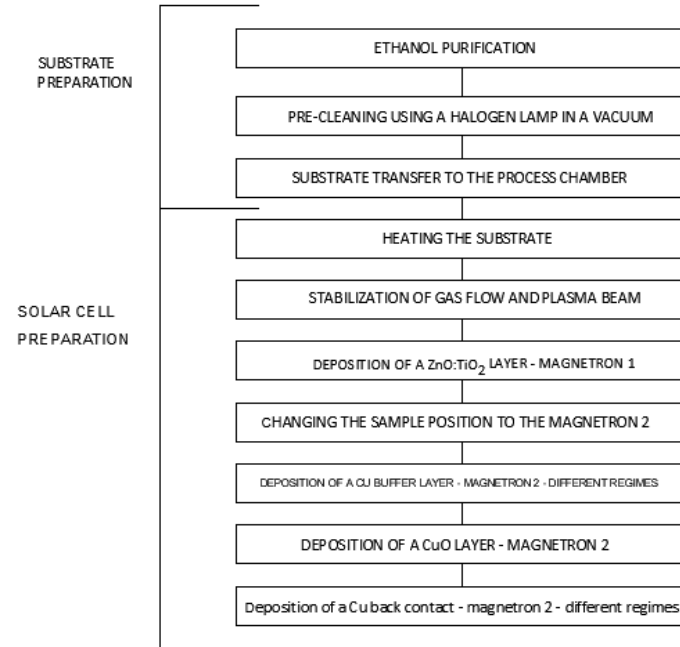


Figure 2. Process flow diagram for the production of TiO₂:ZnO/CuO solar cells.

Additionally, for Sample #26, an initial Ti layer was deposited by 5 s at 1 cm³/s and an argon flow was applied. The oxygen flow was then set at 30%, and the TiO₂ growth started smoothly. To create a photovoltaic device, two Cu contacts were attached to the upper Cu electrode and the ITO using silver conductive glue.

3. Results

3.1. Theoretical Calculations of the Electronic Properties of $\text{TiO}_2/\text{ZnO}/\text{CuO}$

Based on the first-principles calculations, we investigated the electronic properties of the TiO_2/ZnO film doped with Cu and CuO atoms. The results were obtained using a software code [22] that implemented the Car–Parinello quantum mechanical dynamics using a local approximation of the electron density function [23] and a pseudopotential preserving norm from the first principles of Bechele, Hemann, and Schleiter [24].

In this work, we created a cubic structure of the $\text{Fm}\bar{3}\text{m}$ space group for the aforementioned film system. The lattice constants were: TiO_2 (4.84 Å), ZnO (4.63 Å), Cu (3.62 Å), CuO (4.23 Å). For further calculations, we took the value of the total lattice constant of 4.33 Å as the arithmetic mean among the values of the lattice constants presented.

To reproduce the infinite TiO_2/ZnO film doped with Cu/CuO, atomic bases of primitive superlattices cells were created that consisted of successive atomic layers of TiO_2 , ZnO , Cu, and CuO relative to the direction of the coordinate axis OZ, as shown in Figure 3f. At the same time, the parameters of the cell were such that in the X and Y directions it was possible to simulate an infinite surface of the film, and free surfaces (100) with a passivating coating in the Z direction.

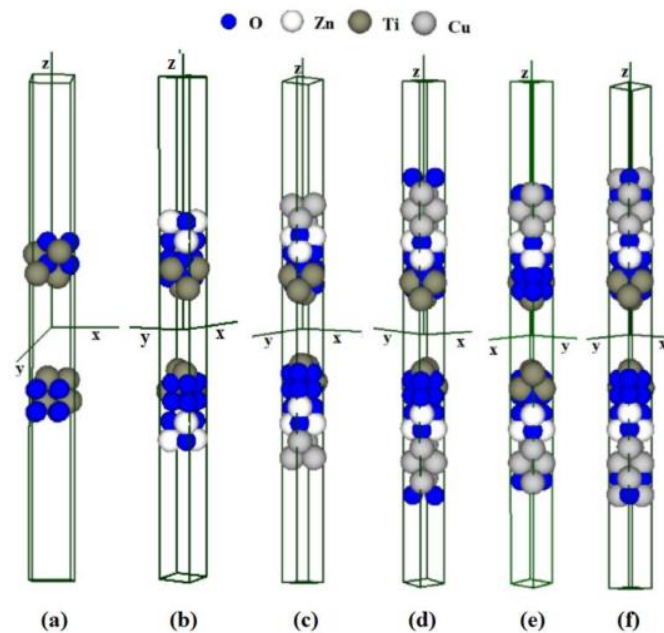


Figure 3. Mechanism of doping the TiO_2/ZnO (100) film system with Cu/CuO atoms: (a) TiO_2 film; (b) TiO_2 film doped with ZnO; (c) TiO_2/ZnO film system with absorbed Cu; $\text{TiO}_2/\text{ZnO}/\text{Cu}$ film system with an absorbed O_2 molecule ((d) above Cu atoms (100); (e) in the interatomic void of Cu atoms (100)); and (f) TiO_2/ZnO (100) film system doped with Cu/CuO atoms.

To study the mechanism of dissociation of Cu/CuO molecules on the surface of (100) TiO_2/ZnO , we created four calculation models: (1) TiO_2 film; (2) TiO_2 film doped with ZnO; (3) TiO_2/ZnO film system with absorbed Cu; and (4) $\text{TiO}_2/\text{ZnO}/\text{Cu}$ film system with an absorbed O_2 molecule (above Cu (100) atoms; in the interatomic void of Cu (100) atoms).

We obtained the distributions of valence electrons from the energy bands for the Cu/CuO-doped TiO_2/ZnO film system. Figure 4 shows the distribution of electrons in energy zones for the G state. At the same time, the horizontal axis shows the deposited energy in atomic units, and the vertical axis shows the number of states per elementary energy interval.

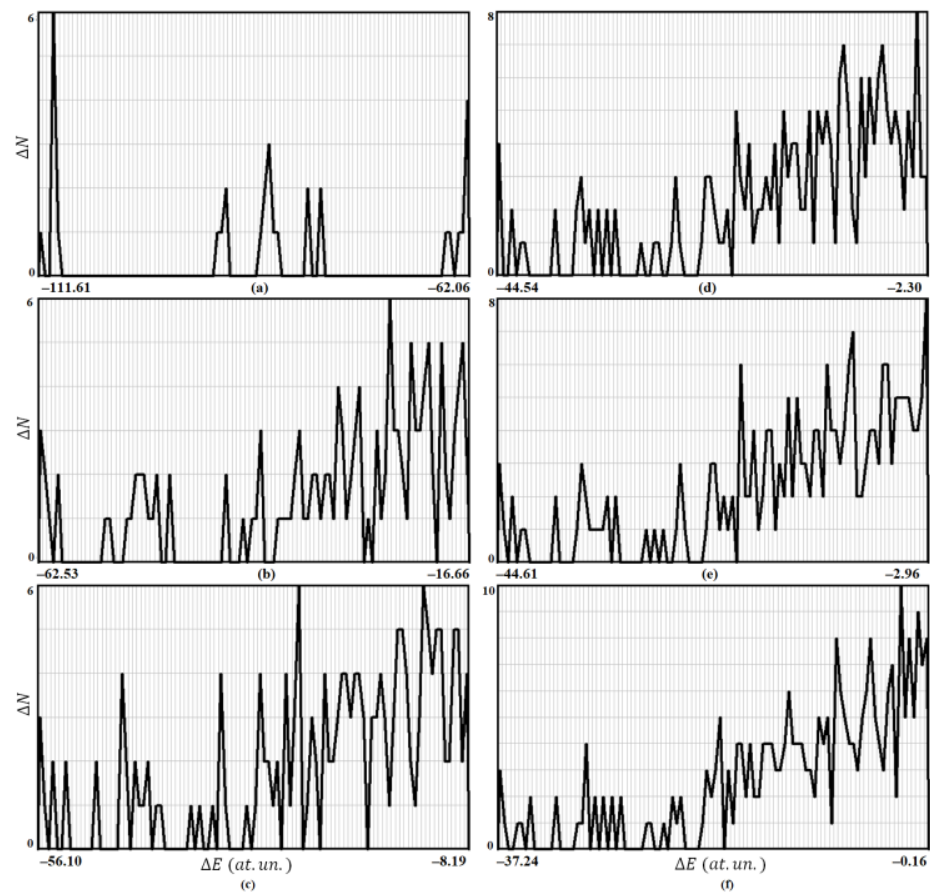


Figure 4. Distribution of valence electrons by energy bands for the Cu/CuO doped TiO₂/ZnO film system: (a) TiO₂ film; (b) TiO₂ film doped with ZnO; (c) TiO₂/ZnO film system with adsorbed Cu; the surface of TiO₂/ZnO/Cu with an adsorbed O₂ molecule (above Cu atoms (100) (d); in the interatomic void of Cu atoms (100) (e)); (f) TiO₂/ZnO (100) film system doped with Cu/CuO atoms. The number of states is plotted on the vertical axis, and the energy range in atomic units is plotted on the horizontal axis.

According to Figure 4, the minimum range of the TiO₂/ZnO film system doped with Cu/CuO corresponds to the value from $E = -37.24$ at.un. to $E = -0.16$ at.un. with the maximum population of states of the valence band 10 (Figure 4f). The maximum energy value corresponds to a pure TiO₂ film with an energy range from $E = -111.61$ at.un. to $E = -62.06$ at.un. The maximum occupancy of the valence band states is equal to 6 (Figure 4a). The number of allowed states was determined by half the number of electrons (electron spin was not taken into account). Comparing Figure 4b,f, we also observe a decrease in the energy of the film system and an increase in the maximum occupancy of the valence band states. As we can see, doping the film with Cu/CuO atoms of the TiO₂/ZnO film system leads to an improvement in the internal properties of the binary oxides.

At the same time, analyzing Figure 4d,e, it can be concluded that the absorption of an oxygen molecule on the surface of TiO₂/ZnO/Cu is more likely in the interatomic void of Cu (100) atoms (Figure 4e). In this case, the energy range takes the value from $E = -44.54$ at.un. to $E = -2.30$ at.un. The maximum occupancy of the valence band states is equal to 8.

3.2. Structure Analysis of the TiO₂:ZnO/CuO Heterostructures

Figure 5 shows SEM images of the cross-sectional views of the thin-film heterostructures deposited on the silicon substrates under different technological parameters, according to Tables 1 and 2. The thickness of the n-TiO₂:ZnO and CuO layers was measured

from the SEM images. It can be seen that in Samples #27 and #26 (Figure 5a,b) the first layer of TiO₂:ZnO obtained on (100) silicon substrates was a homogeneous and dense layer. Samples #27 and #26 have clearly defined directions of growth of the CuO layer which are manifested in its columnar structure. At the initial stages of condensation, diffusion growth is preferred, and the islands grow more intensively in the lateral direction, merging with each other, thus increasing the average lateral values (diameters) even more. After the film has developed sufficiently in the lateral direction, there is a transition to a more intense normal growth. In this case, the Wagner growth process already has an advantage. Therefore, the size increases when the duration of the deposition increases as the contribution of the altitude to its total value increases [25,26].

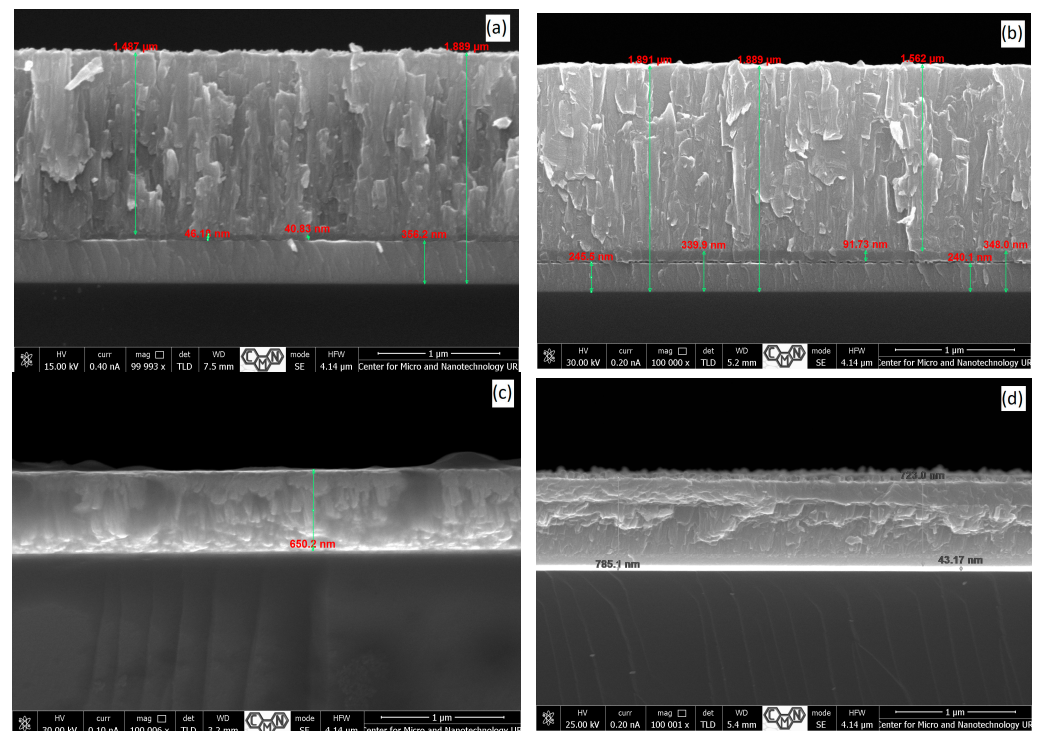


Figure 5. Cross-sectional SEM images of TiO₂:ZnO/CuO thin films obtained at different technological parameters: (a) sample #27, (b) sample #26, (c) sample #18, and (d) sample #15 according to Tables 1 and 2.

However, for Samples #18 and #15, shown in Figure 5c,d, the columnar structure of the CuO layer can still be recognized, though it is less obvious in the cross-sectional images. In discussing these results, it can be assumed that the CuO adatoms, in reaching the surface from the atomic pair formed from the source (Cu target), carry out random wandering (i.e., surface diffusion) on the surface.

The first stage of the growth of the TiO₂:ZnO film is the formation of clusters (stage of homogeneous and/or heterogeneous nucleation, Figure 5c,d). The characteristics of this stage are of primary importance for establishing the structural properties (defects, stress, etc.) of the finally grown film after the general deposition process. At this stage of nucleation, the surface density of the adatoms is very low, and therefore atomic interaction occurs mainly between adatoms and substrate atoms. However, at this stage, the adatoms deposited on the surface also interact with new atoms that are constantly arriving from the vapor phase during deposition. Based on this, such an interaction becomes a competitive phenomenon for the surface diffusion process of adatoms: the final morphology of the film will ultimately be determined by the competition between the surface diffusion of adatoms and the rate of arrival of atoms from the vapor phase [27].

3.3. I-V Characteristics and Parameters Measurement

To verify the quality of the final sample, I-V measurements were performed at AM 1.5 STC. From the complete set of obtained samples, only the photovoltaic parameters of cells #26 and #27 are presented in Table 3. The rest of the experiments did not provide samples with a noticeable photovoltaic effect and were omitted.

Table 3. Photovoltaic parameters of two selected samples: #26 and #27.

Parameter	Sample #26	Sample # 27
Total cells area [cm ²]	0.7	
V _{OC} [mV]	15	11
I _{SC} [uA]	6.8	6.1
P _{max} [nW]	28.65	20.61
η [%]	0.0512×10^{-3}	0.037×10^{-3}
FF [%]	28	31
R _{sh} [k Ω]	2.2	1.8
R _s [k Ω]	1.88	1.36

Figure 6 presents the I-V characteristics of both cells with their approximations and some reference to a possible explanation of the phenomenon. Any specific comments on these results are presented in the discussion section.

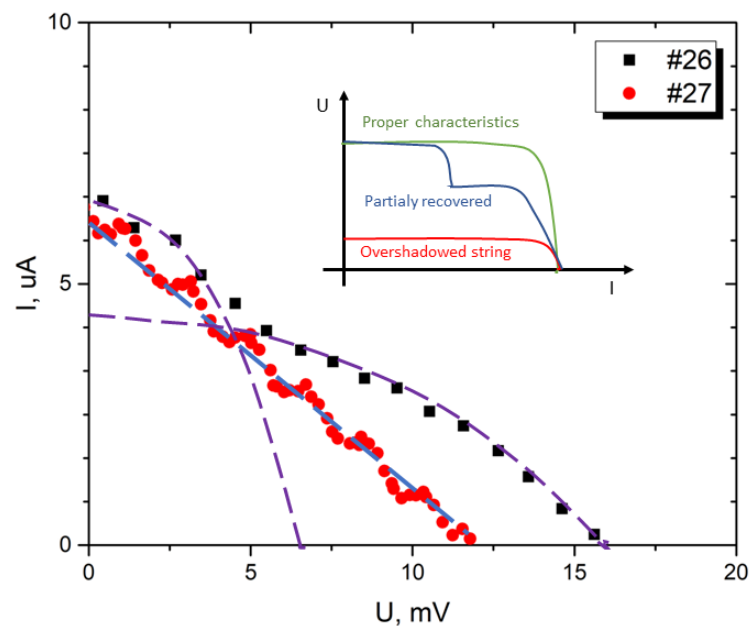


Figure 6. Current–voltage characteristics of Samples #26 and #27 with their proposed approximations. Subgraph [own diagram based on Ref. [28]] presents a possible explanation of the behavior of the characteristics.

The electrical parameters of the selected cells were measured directly and recalculated to obtain FF, efficiency, and resistance values. A specific analysis of the parameters and a possible explanation of the observed phenomenon are provided in the Discussion section. To illustrate sample behavior, I-V characteristics and their approximations are provided in Figure 6.

3.4. Optical Properties of Heterostucture TiO₂:ZnO/CuO

Reflection spectra studies were carried out for Samples #15, #18#, 26, and #27, measured from the side of the CuO layer. Spectra in the range of 200–2500 nm are shown in Figure 7.

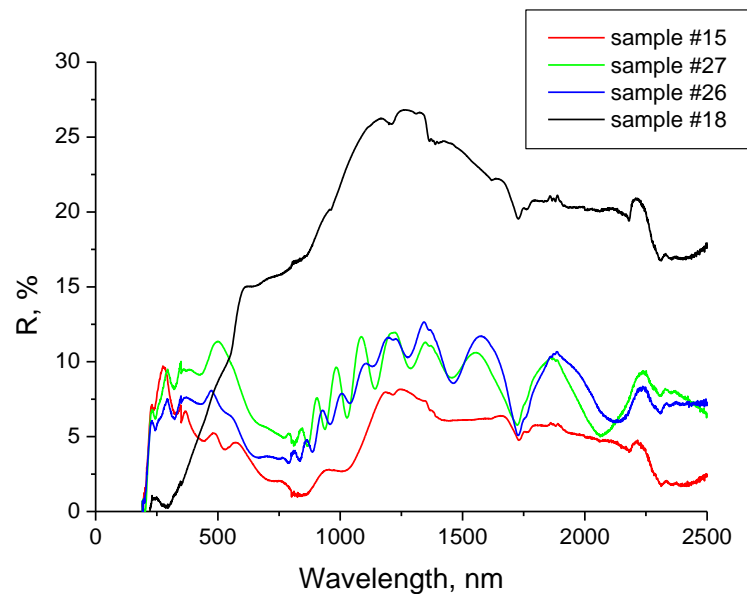


Figure 7. Reflection spectra of samples #15, #18#, #26, and 27 in the wavelength range of 200–2500 nm.

The reflectance varied from 0–27% depending on the wavelength and sample. Reflectance spectra will vary between samples, with the smallest differences for Samples #26 and #27. Strong interference bands are visible in the reflection spectra of Samples #26 and #27, especially in the infrared region.

4. Discussion

Taking into the results presented, one may evaluate the complexity of the layer-formation process on the TiO₂:ZnO/CuO solar cell and the influence of the process flow on Cu diffusion and the final structure behavior.

To study the electronic properties of the TiO₂/ZnO film doped with Cu and CuO atoms, we obtained distributions of valence electrons by energy bands for the cubic structure of the space group Fm $\bar{3}$ m.

It was established that doping the film with Cu/CuO atoms of the TiO₂/ZnO film system led to an improvement in the internal properties of the binary oxides. At the same time, the absorption of an oxygen molecule on the TiO₂/ZnO/Cu surface was more likely in the interatomic void of Cu (100) atoms. The results obtained allow for a deeper understanding and control of the optimization of TiO₂/ZnO thin-film systems.

Based on the structural analyses of Samples #18 and #15, shown in Figure 5c,d, the columnar structure of the CuO layer can still be recognized but is less obvious in the cross-sectional images. This diffusion can be quantitatively described using the surface diffusion coefficient $D = D_0 \exp[-E_A/kT]$ (D and D_0 measured in m²/s, and E_A in J (or eV) so as kT), where D_0 (the preexponential factor) is related to the frequency of attempts by the adatoms to jump from one surface site to another, E_A is the activation energy of the jump phenomenon, k is the Boltzmann constant, and T is the absolute temperature at which the adatom jump process occurs [27,29]. Key factors in establishing the activation energy are, for example, the interatomic energy between adatoms and substrate atoms and between the adatoms themselves. Surface diffusion is one of the most important processes in crystal growth. On a crystallographically singular surface, arriving atoms are not directly incorporated into the crystal. Rather, they migrate on the surface until they are incorporated into the crystal or evaporate to the vapor phase [30,31].

Owing to a proper crystallographic structure created by column grain growth, Samples #26 and #27 achieved a detectable photovoltaic effect. Both of these samples presented low electric parameters; however, the characteristic flow of these samples was very in-

teresting according to the possible construction issues, which may be addressed in the forthcoming research.

Sample #27 presented uniform, flat characteristics with an FF value close to 25%. This was due to the high value of series resistance caused by the poor electrical contact of the inner layers and some problems with the effective ohmic contact with the electrodes. This resulted in very limited Voc (11 mV) and Isc (6.5 μ A) values.

More interesting are the results presented by Sample #26. Observing the I-V characteristics apart from the visible photovoltaic effect with the functioning p-n junction, one may distinguish two sectors of the curve. For the lower voltage part (Part 1) the FF may be calculated at the value of 50%, whereas in the higher voltage range (Part2), the FF was equal to 45%. Part 1 additionally presents a lower value of series resistance and a higher value of shunt resistance, whereas the Rsh in total was 20% higher than in Sample 27 and the Rs was more than 30% higher as well. This phenomenon is similar to the overshadowing of a single cell in a series string (sub-graph). This observation leads to a conclusion of non-homogeneity within the structure which must be further explored. Providing the homogenous characteristic flow of Sample #26, one may expect at least a 20% higher Rsh and a 30–50% lower Rs value. Under these conditions, the expected FF may achieve a value of 50–55%. All observed phenomena originated from the deposition process conditions and also influenced the specific carrier concentrations and mobilities, which will be further investigated.

The good directional ordering of the crystallites in the structure of layers #26 and #27 was confirmed by the appearance of interference bands in the reflection spectrum, which appear when the surface of the layer reflects light without much scattering or absorption over most of the surface of the layer. In addition, the interference patterns observed in the optical reflectance spectra were an indication for the thickness homogeneity of the deposited films [32].

The difference in reflection spectra between Samples #26 and #27 and #15 and #18 may be the result of their structure—for layers #26 and #27, columnar growth was observed which was hardly visible for the other two layers.

The low value of the reflectance coefficient means that a thin CuO layer can also be used as an anti-reflective coating on the solar cell [33]. Differences in reflectance between samples #15, #26, and #27 can be partially explained by layer thickness, with reflectance generally increasing with layer thickness, inversely as in work [34]. Sample #18 clearly differed from the others in the value of the reflectance coefficient. It was relatively large, which may be due to the surface structure resembling a solid, smooth mirror layer (Figure 5c).

5. Conclusions

A complex analysis of the TiO₂:ZnO/CuO structure performance in the dependence on the Cu diffusion in layer formation process was prepared. The photoelectric effect was achieved in two samples. Structure #26 looks more promising, but some serious shortcomings should be eliminated before scaling up the experiments. Firstly, the high, serious resistance present in both structures must be eliminated by improving their interlayer and electrode contacts. Then, it is necessary to eliminate the visible inconsistency, similar to shading in the connection of the photovoltaic string (strip). This can be achieved due to the homogeneity of the serial connection between the manufactured semiconductor layers. It was confirmed that the presence of a Cu buffer layer and a smooth start to the deposition process of the CuO layer play a beneficial role in the cell-manufacturing procedure. Samples #26 and #27, which are characterized by columnar growth, have a high optical surface quality manifested by numerous interference patterns in the reflection spectrum. The uniformity of the thickness of the layers is also evidenced by interference patterns. Structural improvements in the manufactured junctions and the contact point system may lead to higher overall coherence in this area of study. In order to improve the efficiency of the discussed cells, the authors plan to study the influence of different types of ITO layers on the growth mechanisms of the TiO₂:ZnO layer and TiO₂:ZnO/Cu_xO solar cells;

study the influence of silver nanoparticles on the efficiency of cells [35]; test the impact of the contact technique used; and test the feasibility of making ultra-thin TiO₂:ZnO/Cu_xO solar cells.

Supplementary Materials: The authors invite readers to view a YouTube video of the PREVAC apparatus, PVD laboratory, and SCAPS simulations, which are linked below: Link I: <https://www.youtube.com/watch?v=-0Sn4UbiKaE> (accessed on 12 February 2023); Link II: <https://www.youtube.com/watch?v=Lavsm1CIqhY> (accessed on 12 February 2023); Link III: <https://www.youtube.com/watch?v=iei5bn2UAzg\046t=35s> (accessed on 12 February 2023); Link IV: <https://www.youtube.com/watch?v=0TjWJwxLZYk\046t=4s> (accessed on 12 February 2023); Link V: <https://www.youtube.com/watch?v=2eVuIOQxFWw&t=47s>. (accessed on 12 February 2023).

Author Contributions: G.W.: Sample preparation, formal analysis, writing—Review & editing, conceptualization, supervision, and software. P.S.-C.: conceptualization, writing—original draft, project administration, and supervision. A.W.: writing—original draft, writing—review & editing, and supervision. M.S.: writing—original draft, P.P.: writing—original draft, R.Y.: writing—original draft, L.N.: writing—original draft, D.P.: methodology, M.B.: visualization, methodology, M.C.: supervision and writing—original draft, O.M.C. All authors have read and agreed to the published version of the manuscript.

Funding: This research received no external funding.

Institutional Review Board Statement: Not applicable.

Informed Consent Statement: Not applicable.

Data Availability Statement: The data presented in this study are available on request from the corresponding author.

Conflicts of Interest: The authors declare no conflict of interest.

References

- Bracht, H. Copper related diffusion phenomena in germanium and silicon. *Mater. Sci. Semicond. Process.* **2004**, *7*, 113–124. [CrossRef]
- Rha, S.K.; Lee, W.J.; Lee, S.Y.; Hwang, Y.S.; Lee, Y.J.; Kim, D.I.; Kim, D.W.; Chun, S.S.; Park, C.O. Improved TiN film as a diffusion barrier between copper and silicon. *Thin Solid Film.* **1988**, *320*, 134–140. [CrossRef]
- Wang, M.T.; Lin, Y.C.; Chen, M.C. Barrier Properties of Very Thin Ta and TaN Layers Against Copper Diffusion. *J. Electrochem. Soc.* **1998**, *145*, 2538–2545. [CrossRef]
- Laurila, T.; Zeng, K.; Kivilahti, J.K.; Molarius, J.; Suni, I. TaC as a diffusion barrier between Si and Cu. *J. Appl. Phys.* **2002**, *91*, 5391–5399. [CrossRef]
- Byrne, C.; Brennan, B.; McCoy, A.P.; Bogan, J.; Brady, A.; Hughes, G. In Situ XPS Chemical Analysis of MnSiO₃ Copper Diffusion Barrier Layer Formation and Simultaneous Fabrication of Metal Oxide Semiconductor Electrical Test MOS Structures. *ACS Appl. Mater. Interfaces* **2016**, *8*, 2470–2477. [CrossRef] [PubMed]
- An, B.-S.; Kwon, Y.; Oh, J.-S.; Lee, C.; Choi, S.; Kim, H.; Lee, M.; Pae, S.; Yang, C.-W. Characteristics of an Amorphous Carbon Layer as a Diffusion Barrier for an Advanced Copper Interconnect. *ACS Appl. Mater. Interfaces* **2020**, *12*, 3104–3113. [CrossRef]
- Li, Z.; Tian, Y.; Teng, C.; Cao, H. Recent advances in barrier layer of Cu interconnects. *Materials* **2020**, *13*, 5049. [CrossRef]
- Aiello, A.F. Investigation of a Self-Assembled Monolayer as a Cu Diffusion Barrier for Solar Cell Metallization. *J. Microelectron. Eng. Conf.* **2014**, *20*, 6–10.
- Peterson, N.L.; Wiley, C.L. Diffusion and point defects in Cu₂O. *J. Phys. Chem. Solids* **1984**, *45*, 281–294. [CrossRef]
- Moore, W.J.; Selikson, B. The Diffusion of Copper in Cuprous Oxide. *J. Chem. Phys.* **1951**, *19*, 1539–1543, Erratum in *J. Chem. Phys.* **1952**, *20*, 927. [CrossRef]
- Tomlinson, W.J.; Yates, J. The diffusion of Cu in copper(i) oxide. *J. Phys. Chem. Solids* **1977**, *38*, 1205–1206. [CrossRef]
- Iguchi, E.; Yajima, K.; Saito, Y. Oxidation Kinetics of Cu to Cu₂O. *Trans. Jpn. Inst. Met.* **1973**, *14*, 423–430. [CrossRef]
- Maack, B.; Nilius, N. Morphological and Kinetic Insights into Cu₂O–CuO Oxidation. *Phys. Status Solidi Basic Res.* **2020**, *257*, 1900365. [CrossRef]
- Unutulmazsoy, Y.; Cancellieri, C.; Lin, L.; Jeurgens, L.P.H. Reduction of thermally grown single-phase CuO and Cu₂O thin films by in-situ time-resolved XRD. *Appl. Surf. Sci.* **2022**, *588*, 152896. [CrossRef]
- Lee, S.K.; Hsu, H.C.; Tuan, W.H. Oxidation behavior of copper at a temperature below 300 °C and the methodology for passivation. *Mater. Res.* **2016**, *19*, 51–56. [CrossRef]
- Zuo, C.; Ding, L. Solution-Processed Cu₂O and CuO as Hole Transport Materials for Efficient Perovskite Solar Cells. *Small* **2015**, *11*, 5528–5532. [CrossRef]

17. Rahaman, R.; Sharmin, M.; Podder, J. Band gap tuning and p to n-type transition in Mn-doped CuO nanostructured thin films. *J. Semicond.* **2022**, *43*, 012801. [[CrossRef](#)]
18. El-Hadary, M.I.; Senthilraja, S.; Zayed, M.E. A hybrid system coupling spiral type solar photovoltaic thermal collector and electrocatalytic hydrogen production cell: Experimental investigation and numerical modelling. *Process Saf. Environ. Prot.* **2023**, *170*, 1101–1120. [[CrossRef](#)]
19. Elaziz, M.A.; Senthilraja, S.; Zayed, M.E.; Elsheikh, A.H.; Mostafa, R.R.; Lu, S. A new random vector functional link integrated with mayfly optimization algorithm for performance prediction of solar photovoltaic thermal collector combined with electrolytic hydrogen production system. *Appl. Therm. Eng.* **2021**, *193*, 117055. [[CrossRef](#)]
20. Košiček, M.; Zavašnik, J.; Baranov, O.; ŠetinaBatič, B.; Cvelbar, U. Understanding the Growth of Copper Oxide Nanowires and Layers by Thermal Oxidation over a Broad Temperature Range at Atmospheric Pressure. *Cryst. Growth Des.* **2022**, *22*, 6656–6666. [[CrossRef](#)]
21. Wisz, G.; Sawicka-Chudy, P.; Wal, A.; Potera, P.; Bester, M.; Płoch, D.; Sibiński, M.; Cholewa, M.; Ruszała, M. TiO₂:ZnO/CuO thin film solar cells prepared via reactive direct-current (DC) magnetron sputtering. *Appl. Mater. Today* **2022**, *29*, 101673. [[CrossRef](#)]
22. Ab Initio Calculation. Available online: <http://sites.google.com/a/kdpu.edu.ua/calculationphysics/> (accessed on 3 February 2023).
23. Kohn, W.; Sham, L.J. Self-Consistent Equations Including Exchange and Correlation Effects. *Phys. Review.* **1965**, *140*, A1133–A1138. [[CrossRef](#)]
24. Bachelet, G.B.; Hamann, D.R.; Schlüter, M. Pseudopotentials That Work: From H to Pu. *Phys. Rev. B* **1982**, *26*, 4199–4228. [[CrossRef](#)]
25. Saliy, Y.P.; Nykyruy, L.I.; Yavorskyi, R.S.; Adamiak, S. The Surface Morphology of CdTe Thin Films Obtained by Open Evaporation in Vacuum. *J. Nano- Electron. Phys.* **2017**, *9*, 410–416. [[CrossRef](#)]
26. Wagner, C. Theorie der Alterung von Niederschlagen durch Umlösen (Ostwald Reifung). *Zs. Electrochem.* **1961**, *65*, 581–591.
27. Ruffino, F.; Grimaldi, M.G. Morphological Characteristics of Au Films Deposited on Ti: A Combined SEM-AFM Study. *Coatings* **2018**, *8*, 121. [[CrossRef](#)]
28. Pei, T.; Hao, X. A Fault Detection Method for Photovoltaic Systems Based on Voltage and Current Observation and Evaluation. *Energies* **2019**, *12*, 1712. [[CrossRef](#)]
29. Tu, K.N.; Mayer, J.W.; Feldman, L.C. *Electronic Thin Film Science*; Macmillan Publishing Company: New York, NY, USA, 1992; Ruffino, F.; Torrisi, V. Ag films deposited on Si and Ti: How the film-substrate interaction influences the nanoscale film morphology. *Superlatt. Microstruct.* **2017**, *111*, 81–89.
30. Yavorskyi, R. Features of optical properties of high stable CdTe photovoltaic absorber layer. *Phys. Chem. Solid State* **2020**, *21*, 243–253. [[CrossRef](#)]
31. Tatau, N.; Kuech, T.F. *Handbook of Crystal Growth: Thin Films and Epitaxy. Materials, Processes, and Technology*; Elsevier: Amsterdam, The Netherlands, 2015.
32. Punitha, K.; Sivakumar, R.; Sanjeeviraja, C.; Sathe, V.; Ganesan, V. Physical properties of electron beam evaporated CdTe and CdTe:Cu thin films. *J. Appl. Phys.* **2014**, *116*, 213502. [[CrossRef](#)]
33. Wanjala, K.S.; Njoroge, W.K.; Makori, N.E.; Ngaruiya, J.M. Optical and Electrical Characterization of CuO Thin Films as Absorber Material for Solar Cell Applications. *Am. J. Condens. Matter Phys.* **2016**, *6*, 1–6. [[CrossRef](#)]
34. Hussein, H.A.; Al-Mayaleeb, K.H. Study the Effect of Thickness on the Optical Properties of Copper Oxide Thin Films by FDTD Method. *Turk. J. Comput. Math. Educ.* **2021**, *12*, 3865–3870.
35. Wisz, G.; Potera, P.; Sawicka-Chudy, P.; Gwóźdź, K. Optical Properties of ITO/Glass Substrates Modified by Silver Nanoparticles for PV Applications. *Coatings* **2023**, *13*, 61. [[CrossRef](#)]

Disclaimer/Publisher’s Note: The statements, opinions and data contained in all publications are solely those of the individual author(s) and contributor(s) and not of MDPI and/or the editor(s). MDPI and/or the editor(s) disclaim responsibility for any injury to people or property resulting from any ideas, methods, instructions or products referred to in the content.